



**HAL**  
open science

## Precision Measurements of Beta Spectra using Metallic Magnetic Calorimeters within the European Metrology Research Project MetroBeta

Martin Loidl, J. Beyer, L. Bockhorn, J. Bonaparte, C. Enss, S. Kempf, K. Kossert, Riham Mariam, O. Nähle, M. Paulsen, et al.

► **To cite this version:**

Martin Loidl, J. Beyer, L. Bockhorn, J. Bonaparte, C. Enss, et al.. Precision Measurements of Beta Spectra using Metallic Magnetic Calorimeters within the European Metrology Research Project MetroBeta. *Journal of Low Temperature Physics*, 2020, 199 (1-2), pp.451-460. 10.1007/s10909-020-02398-2 . cea-04567222

**HAL Id: cea-04567222**

**<https://cea.hal.science/cea-04567222>**

Submitted on 3 May 2024


**HAL** is a multi-disciplinary open access archive for the deposit and dissemination of scientific research documents, whether they are published or not. The documents may come from teaching and research institutions in France or abroad, or from public or private research centers.

L'archive ouverte pluridisciplinaire **HAL**, est destinée au dépôt et à la diffusion de documents scientifiques de niveau recherche, publiés ou non, émanant des établissements d'enseignement et de recherche français ou étrangers, des laboratoires publics ou privés.



Author Proof

1 **Precision Measurements of Beta Spectra using Metallic**  
2 **Magnetic Calorimeters within the European Metrology**  
3 **Research Project MetroBeta**

4 **M. Loidl<sup>1</sup>  · J. Beyer<sup>2</sup> · L. Bockhorn<sup>3,5</sup> · J. J. Bonaparte<sup>4</sup> · C. Enss<sup>4</sup> · S. Kempf<sup>4</sup> ·**  
5 **K. Kossert<sup>3</sup> · R. Mariam<sup>1</sup> · O. Nähle<sup>3</sup> · M. Paulsen<sup>2,4</sup> · P. Ranitzsch<sup>3</sup> ·**  
6 **M. Rodrigues<sup>1</sup> · M. Wegner<sup>4</sup>**

7 Received: 19 July 2019 / Accepted: 8 February 2020  
8 © Springer Science+Business Media, LLC, part of Springer Nature 2020

9 **Abstract**

10 MetroBeta, a recently completed European Metrology Research Project, aimed at  
11 the improvement of the knowledge of the shapes of beta spectra, both in terms of  
12 theoretical calculation and measurement. The most prominent experimental work  
13 package concerned the measurement of the spectrum shapes of several beta decay-  
14 ing radionuclides by means of metallic magnetic calorimeters (MMCs) with the beta  
15 emitter embedded in the absorber. New MMC chips were designed and optimized  
16 for five different absorber heat capacities, enabling the measurement of beta spectra  
17 with  $Q$  values ranging from few tens of keV up to ~1 MeV. Several beta spectra  
18 were measured with high energy resolution and statistics of up to  $10^7$  counts. A01  
A02

19 **Keywords** Beta spectrometry · Metallic magnetic calorimeter · Radionuclide  
20 metrology

A1 ✉ M. Loidl  
A2 martin.loidl@cea.fr

A3 <sup>1</sup> CEA, LIST, Laboratoire National Henri Becquerel (LNE-LNHB), CEA-Saclay,  
A4 91191 Gif Sur Yvette Cedex, France

A5 <sup>2</sup> Physikalisch-Technische Bundesanstalt (PTB), Abbestrasse 2-12, 10587 Berlin, Germany

A6 <sup>3</sup> Physikalisch-Technische Bundesanstalt (PTB), Bundesallee 100, 38116 Brunswick, Germany

A7 <sup>4</sup> Kirchhoff-Institute for Physics, Heidelberg University, Im Neuenheimer Feld 227,  
A8 69120 Heidelberg, Germany

A9 <sup>5</sup> Present Address: Institut für Festkörperphysik - Abteilung Nanostrukturen, Gottfried Wilhelm  
A10 Leibniz Universität Hannover, 30167 Hannover, Germany

## 21 1 Introduction

22 There are several fields, including radionuclide metrology, nuclear medicine and the  
 23 nuclear power industry, that request improved knowledge of beta spectrum shapes.  
 24 In principle, there are two ways to determine the shapes of beta spectra: theoreti-  
 25 cal calculation or experimental beta spectrometry. Calculations of spectra from  
 26 forbidden, in particular, non-unique transitions are very complicated, and spectra  
 27 published in the literature often reveal large discrepancies for one and the same  
 28 radionuclide. The theoretical approaches for improved calculations must be verified  
 29 against precise experimental data.

30 Metallic magnetic calorimeters (MMCs) with beta emitters enclosed in noble  
 31 metal absorbers have demonstrated their potential for the study of beta spectrum  
 32 shapes [1–3]. In the European Metrology Research Project MetroBeta [4], MMCs  
 33 were optimized for the requirements in beta spectrometry, and three beta spectra  
 34 covering different types of beta transition have been measured:  $^{14}\text{C}$  (allowed),  $^{151}\text{Sm}$   
 35 (first forbidden non-unique) and  $^{99}\text{Tc}$  (second forbidden non-unique). Measurements  
 36 of  $^{36}\text{Cl}$  (second forbidden non-unique) are under way.

## 37 2 Experimental

### 38 2.1 MMC beta Spectrometry System

39 The development of MMCs within the project, optimized for absorber heat capaci-  
 40 ties ranging from 8 pJ/K to 1.7 nJ/K at 20 mK, has been described in Ref. [5].  
 41 Figure 1 shows the design of the “M size” (110 pJ/K) MMC chip together with a

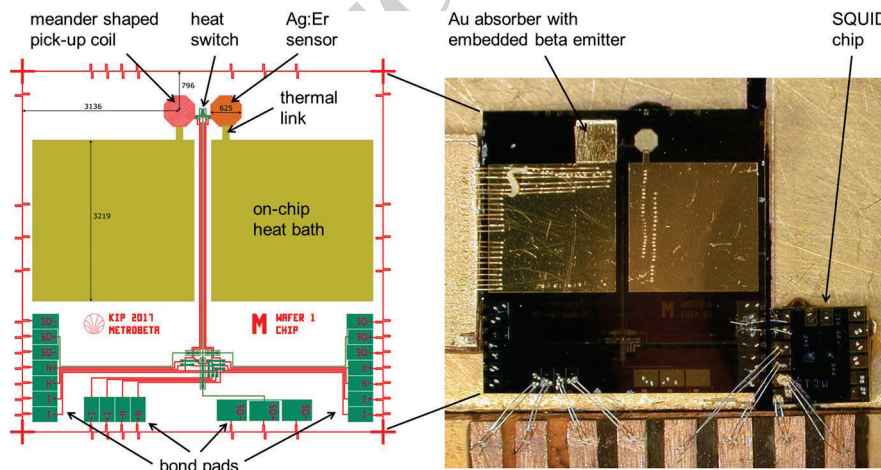


**Fig. 1** *Left:* Design of the “M size” MMC chip. The chip size is  $(7.2 \text{ mm})^2$ . Some additional dimensions are given in the figure in  $\mu\text{m}$ ; the sensor measures  $625 \mu\text{m}$  across. For further details, see Ref. [14]. *Right:* Photograph of a chip from the first fabricated batch; a gold absorber with an embedded beta emitter is placed on one of the Ag:Er sensors. (Color figure online)

42 photograph of a chip from the first fabricated batch. A gold absorber with an embed-  
43 ded beta emitter is visible on one of the two Ag:Er sensors; it was fixed to the sensor  
44 with Stycast 1266 epoxy resin. The SQUID reading out the MMC signal is placed  
45 next to the MMC chip.

## 46 2.2 Source and Absorber Preparation Techniques

47 The source preparation is fundamental for the precise measurement of beta spectra  
48 with MMCs. It must ensure that the entire energy of every beta particle is deposited  
49 and thermalized in the absorber.

50 The best source preparation approach—besides implanting the radionuclide  
51 directly into the absorber material—is electrodeposition forming a metallic layer.  
52 For many elements, however, an oxide/hydroxide layer will form during electrodeposi-  
53 tion. This can still be a high-quality source consisting in a very thin layer. Within  
54 this project,  $^{151}\text{Sm}$  and  $^{99}\text{Tc}$  sources were fabricated by electrodeposition.

55 Where electrodeposition is not possible, as is the case of  $^{14}\text{C}$  or  $^{36}\text{Cl}$ , drop-deposi-  
56 ted sources were produced. The common manual drop deposition often leads to the  
57 formation of large (~micrometers) salt crystals. Previous studies using MMCs have  
58 revealed that salt crystals can cause considerable spectrum distortion due to incom-  
59 plete thermalization [6]. The formation of large salt crystals can be avoided if the  
60 required activity is deposited in a 2D array of very small individual droplets. Com-  
61 mercial micro-dispensing systems can deposit single droplet volumes of less than  
62 50 pl in combination with a placement accuracy of better than 20  $\mu\text{m}$ . With such a  
63 system,  $^{36}\text{Cl}$ ,  $^{99}\text{Tc}$  and  $^{14}\text{C}$  were deposited onto gold foils preformed into absorber  
64 arrays by milling techniques, with lateral dimensions of individual absorber ele-  
65 ments of about 0.7 mm and 1.6 mm. Figure 2a shows an absorber array after the  
66 radioactive solution was dried. Volumes of 100 nl (left half) and 50 nl (right half)  
67 of a  $^{99}\text{Tc}$  solution were deposited in the middle of each marked absorber. The

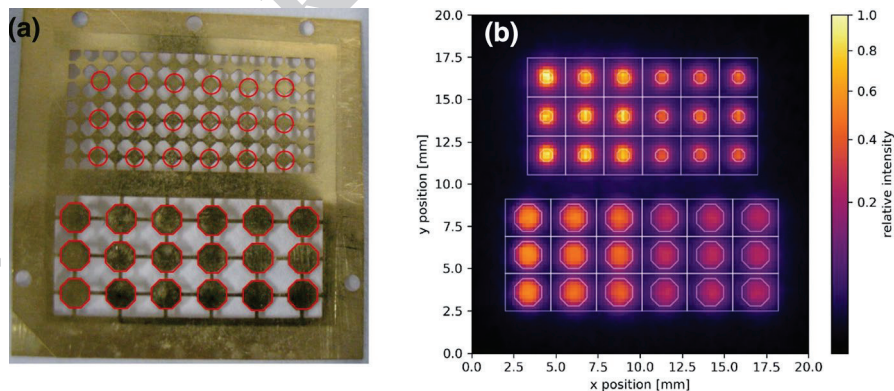


**Fig. 2** **a** Photograph of an array of pre-fabricated gold absorber foils with  $^{99}\text{Tc}$  sources deposited by a microdrop dispenser system in the middle of the marked absorbers. **b** Autoradiography image of the same array. Two different activity levels, 5 Bq/2.5 Bq, have been deposited on each marked absorber in the left/right half of the array. (Color figure online)

68 autoradiography image in Fig. 2b confirms the position and the different activities of  
69 the deposited material.

70 Fine dispersion of the source material in the absorber metal will also improve  
71 the source quality compared to a conventional drop-deposited source. This can be  
72 achieved by alternate folding and laminating of the foil with the source deposit,  
73 breaking the source crystals into tens of nanometer small particles that are embed-  
74 ded in the metal foil [7]. This technique was applied to the electrodeposited  $^{151}\text{Sm}$   
75 source, because it had a black aspect and was considered not to be ideally thin.

76 Monte Carlo simulations—see Sect. 4—indicate that spectrum distortion of  
77 higher energy beta spectra by escape of bremsstrahlung from the absorber can be  
78 reduced by embedding the beta emitter into bilayer absorbers with an inner layer of  
79 lower atomic number and an outer layer of high atomic number (e.g., copper,  $Z=29$ ,  
80 and gold,  $Z=79$ ). Preparing this kind of absorbers requires several steps of diffusion  
81 welding under vacuum or inert gas to avoid oxidation of the copper.

### 82 3 Beta Spectrum Measurements

83 Three beta spectra have been measured using MMCs within the MetroBeta project;  
84 the more challenging  $^{36}\text{Cl}$  measurements are under way.

#### 85 3.1 $^{14}\text{C}$

86 The spectrum of  $^{14}\text{C}$  ( $Q=156.476$  keV) has been measured using a source prepared  
87 as described in Ref. [5]. The absorber (Au,  $1\text{ mm}^2 \times (2 \times 25\text{ }\mu\text{m})$ ) was placed on an **AQ3**  
88 MMC chip best matching its heat capacity (34 pJ/K at 10 mK). The experimen-  
89 tal conditions during the measurement were far from optimal. During the cooling  
90 phase, the glue layer fixing the MMC chip to its holder broke; the chip was then  
91 only suspended by the gold and aluminum bonding wires used for electric and ther-  
92 mal contacts. Hence, the MMC could vibrate, resulting in an energy resolution near  
93 200 eV (FWHM), approximately five times worse than expected from the absorber  
94 heat capacity. Nevertheless, the detector performance was much better than in the  
95 measurement published in [5]: The energy resolution was improved by a factor of  
96 five, while the energy threshold was reduced from  $\sim 5$  to  $\sim 700$  eV. Figure 3 shows  
97 the experimental spectrum containing 2.7 million events together with a theoretical  
98 spectrum calculated with the code BetaShape [8, 9].

#### 99 3.2 $^{151}\text{Sm}$

100 A  $^{151}\text{Sm}$  source was electrodeposited on a 10- $\mu\text{m}$ -thick silver foil, forming a Sm  
101 oxide/hydroxide layer. After the mechanical processing described in Sect. 2.2, this  
102 source foil ( $0.8\text{ mm} \times 0.8\text{ mm} \times 7\text{ }\mu\text{m}$ ) was sandwiched between two silver foils  
103 ( $0.9\text{ mm} \times 0.9\text{ mm} \times 15\text{ }\mu\text{m}$  each, total absorber heat capacity: 14.5 pJ/K at 10 mK).  
104 The performance of the MMC during this measurement was as expected: The

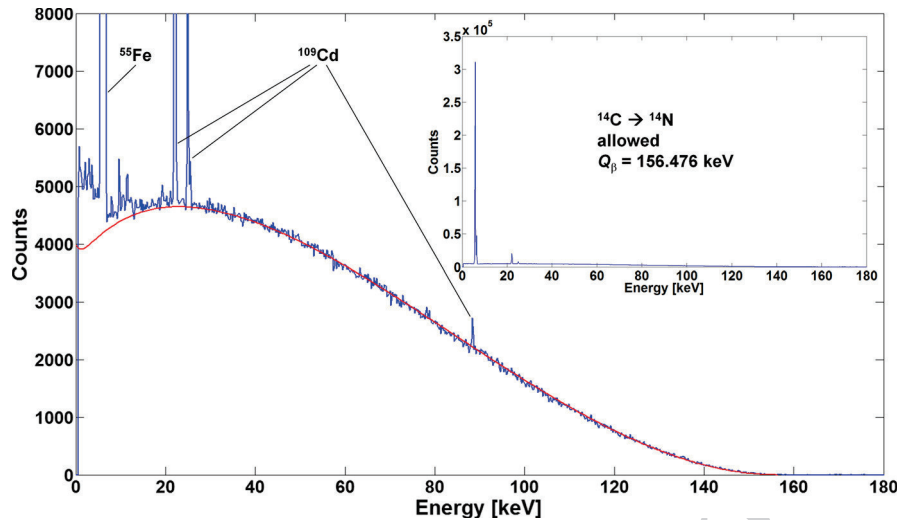


**Fig. 3** Beta spectrum of  $^{14}\text{C}$  measured with an MMC (blue). The discrete lines are X-ray and gamma ray lines from an external  $^{55}\text{Fe} + ^{109}\text{Cd}$  energy calibration source. The inset shows the unclipped spectrum with the energy calibration lines in full height. A theoretical spectrum calculated with the code BetaShape is shown in red. The deviation of the experimental spectrum at low energies may be attributed to the degraded detector performance. (Color figure online)

105 energy resolution ranges from 45 eV (FWHM) at 6 keV to 70 eV at 25 keV, and the  
 106 energy threshold is 250 eV.

107  $^{151}\text{Sm}$  has a main  $\beta^-$  decay branch ( $Q_\beta = 76.4 \text{ keV}$ ) to the ground state and a sec-  
 108 ond  $\beta^-$  decay branch to the 21.54 keV excited level of  $^{151}\text{Eu}$ . The recommended val-  
 109 ues for the probabilities of the two decay paths are 99.07 (4) % and 0.93 (4) % [10].  
 110 The de-excitation of the 21.54 keV excited state leads to the emission of gamma rays  
 111 (3.4% of the decays), respectively, to the emission of conversion electrons and sub-  
 112 sequently X-rays and/or Auger electrons. The detector absorber stops all conversion  
 113 electrons, more than 99% of all X-rays and more than 95% of the 21.54 keV gamma  
 114 photons. The result is that for practically all beta decays to the excited level, the sum  
 115 of the beta energy and the gamma energy is absorbed. Thus, the measured spectrum  
 116 for the decays to the excited level is shifted by the energy of the gamma transition  
 117 and starts at 21.54 keV, leading to a step in the recorded spectrum. Since the maxi-  
 118 mum energy for this beta branch equals the  $Q$  value minus the gamma transition  
 119 energy, the end point of both measured spectra is the same, 76.4 keV. As it is not  
 120 possible to distinguish events from the two decay branches, both spectra are super-  
 121 imposed in one experimental spectrum.

122 The measured spectrum (10.2 million events) is shown in Fig. 4 together with  
 123 theoretical spectra calculated with the code BetaShape for both decay paths. The  
 124 area between the two theoretical spectra, corresponding to the probability of the  
 125 decay to the excited state of  $^{151}\text{Eu}$ , amounts to 2.6% of the total, in clear contradic-  
 126 tion with the recommended value. Concerning the spectrum shape, the discrepancy  
 127 between experiment and theory at low energies is most likely due to an incomplete

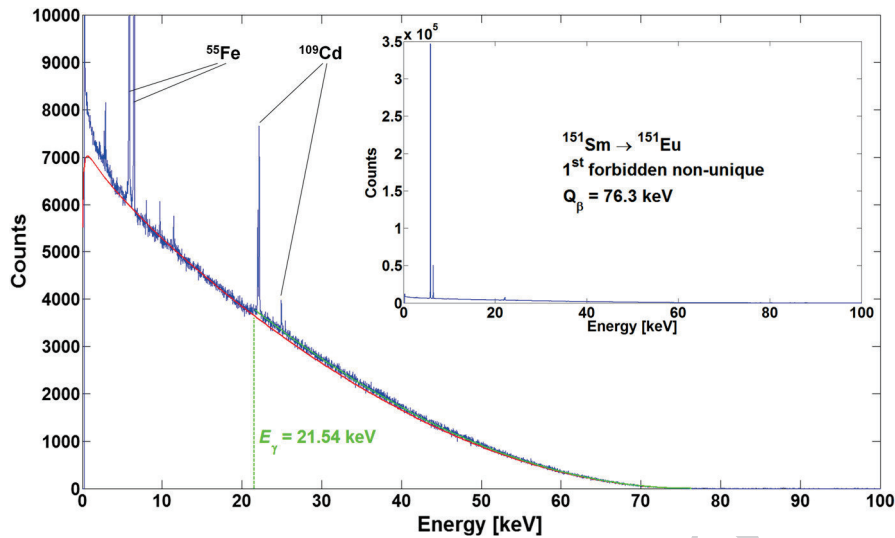


Fig. 4 Beta spectrum of  $^{151}\text{Sm}$  measured with an MMC (blue) together with theoretical spectra calculated for the beta decay to the ground state (red) and to the 21.54 keV excited level of  $^{151}\text{Eu}$  (green). The inset shows the unclipped spectrum with the energy calibration lines in full height. (Color figure online)

128 control of the atomic effects in the theoretical calculation of this first forbidden, non-  
 129 unique transition.

### 130 3.3 $^{99}\text{Tc}$

131 The beta spectrum of  $^{99}\text{Tc}$  ( $Q=293.8$  keV) was measured both at PTB and at LNHB.  
 132 At LNHB, a  $^{99}\text{Tc}$  source was electrodeposited on gold, forming metallic technetium.  
 133 This source foil was sandwiched between two gold foils (0.9 mm $\times$ 0.9  
 134 mm $\times$ 74  $\mu\text{m}$  each,  $C_{\text{abs}}=175$  pJ/K at 10 mK). Data were acquired during 13.7 days,  
 135 and the spectrum contains 5.65 million events. The energy resolution is practically  
 136 energy independent, about 100 eV (FWHM) up to 384 keV, and the highest energy  
 137 gamma line of a  $^{133}\text{Ba}$  source used for energy calibration and check of the linearity.  
 138 Comparing the measured and the tabulated line energies between 31 keV and  
 139 384 keV shows no larger deviations than 70 eV, less than the energy resolution, and  
 140 no obvious trend.

141 At PTB,  $^{99}\text{Tc}$  sources were prepared with a microdrop dispenser directly on a  
 142 90- $\mu\text{m}$ -thick gold absorber array (Fig. 2a). An identical array was diffusion welded  
 143 onto the array with the sources. One of the larger absorbers ( $C_{\text{abs}}=545$  pJ/K at  
 144 20 mK) was glued onto a matching MMC. The spectrum after 42 h of data acquisition  
 145 consists of 0.5 million events with an energy threshold of about 5 keV and an  
 146 energy resolution of 600 eV at the 122 keV gamma line of a  $^{57}\text{Co}$  energy calibration  
 147 source. The larger absorber heat capacity, vibrations from the pulse tube cooler and

148 bath temperature instability explain the degraded energy resolution and threshold  
149 compared to the measurement performed at LNHB.

150 Figure 5 shows a superposition of both experimental spectra; the spectrum  
151 shape is practically the same. The theoretical spectrum that is also shown in Fig. 5  
152 has been calculated with the current version of the code BetaShape, supposing an  
153 allowed transition, and multiplied with an experimental shape factor [11]. It is not  
154 surprising that this shape factor, derived from a measurement with an energy thresh-  
155 old of 55 keV, cannot correctly reproduce the spectrum at lower energies. It is note-  
156 worthy that the spectrum measured at LNHB has an energy threshold of 650 eV.

#### 157 4 Toward the Measurement of $^{36}\text{Cl}$

158 For beta spectra with maximum energies higher than a few 100 keV, potential distortion  
159 of the measured spectra by the escape of bremsstrahlung must be considered. In  
160 first order, the radiative energy loss of the beta particles scales linearly with energy.  
161 Hence, the higher the beta  $Q$  value, the stronger the spectrum distortion will be.  
162 In principle, this distortion can be corrected for via Monte Carlo simulation; how-  
163 ever, the bremsstrahlung cross sections needed for the simulations suffer from high  
164 uncertainties.

165 Since the bremsstrahlung production scales with the square of the atomic num-  
166 ber  $Z$ , a low  $Z$  absorber material may be a good candidate in view of minimizing  
167 this source of spectrum distortion. On the other hand, a low  $Z$  absorber needs to

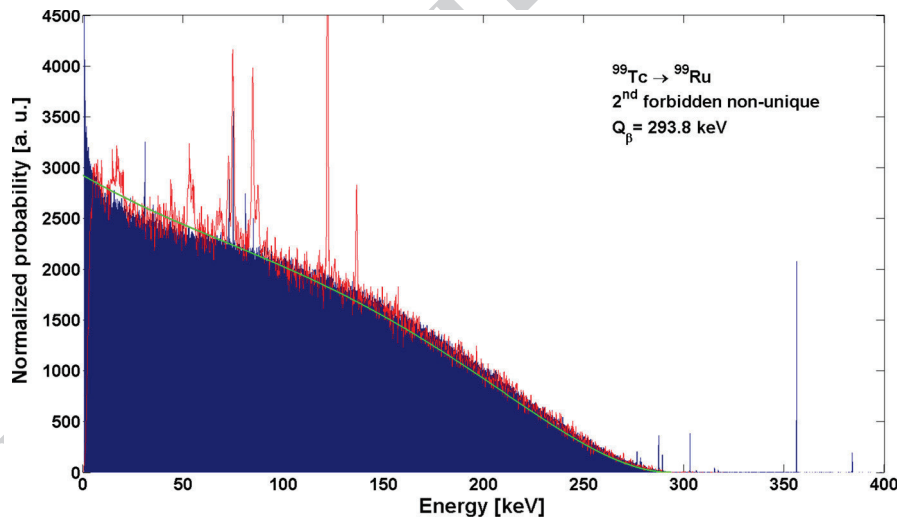


Fig. 5 Beta spectrum of  $^{99}\text{Tc}$  resulting from two fully independent measurements and data analyses. *Blue histogram*: measured at LNHB (Laboratoire National Henri Becquerel, France) and *red line*: measured at PTB (Physikalisch-Technische Bundesanstalt, Germany). All lines in the blue spectrum are from a  $^{133}\text{Ba}$  energy calibration source (including some escape peaks); all lines in the red spectrum are from a  $^{57}\text{Co}$  energy calibration source. A theoretical spectrum calculated with the code BetaShape and using a shape factor from Ref. [11] is also shown (*green*). (Color figure online)



168 be significantly larger in order to stop the beta particles, thus implying larger heat  
169 capacity, and is moreover less efficient for the reabsorption of at least a fraction  
170 of the bremsstrahlung photons. A composite absorber composed of an inner layer  
171 of a low  $Z$  material, reducing the bremsstrahlung production near the beta emitter  
172 where the beta particles have still high energy, and an outer layer of a high  $Z$  mate-  
173 rial, reducing the overall absorber heat capacity compared with a monolithic low  
174  $Z$  absorber and more efficiently reabsorbing photons, may be an interesting option  
175 combining the advantages of both low and high  $Z$ .

176 To test this hypothesis, a series of Monte Carlo simulations have been performed  
177 using the PENELOPE code [12] for the case of  $^{36}\text{Cl}$  ( $Q = 709.53$  keV). Five types of  
178 absorber comprising elements with three different atomic numbers were simulated:  
179 monolithic gold ( $Z = 79$ ), silver ( $Z = 47$ ) and copper ( $Z = 29$ ), and composite absorbers  
180 with an inner copper or silver layer and an outer gold layer. For each absorber  
181 type, in a first step the minimal necessary absorber thickness was determined by  
182 means of lower statistics simulations only at the maximum energy of  $^{36}\text{Cl}$ . In a sec-  
183 ond step, the resulting absorber was simulated with a central 100-nm-thick NaCl  
184 layer acting as a source layer spiked with the active  $^{36}\text{Cl}$ . Electrons with initial ener-  
185 gies following a theoretical spectrum based on the experimental  $^{36}\text{Cl}$  spectrum from  
186 Ref. [1] were generated in the source layer; the result of the simulation is the dis-  
187 tribution of the energies deposited in the absorber, i.e., the expected spectrum that  
188 would be measured with each absorber.

189 Figure 6 presents the five simulated spectra together with the initial theoretical  
190 spectrum. It can be clearly seen that the spectrum distortion is highest for the mono-  
191 lithic gold absorber ( $\sim 1.5\%$  in the energy range 100–200 keV) and becomes smaller  
192 with lower  $Z$ . One can also observe that the spectrum distortion in the composite  
193 silver (resp. copper)–gold absorber is smaller than in the monolithic silver (resp.  
194 copper) absorber. The smallest distortion is obtained with the copper–gold bilayer  
195 absorber.

196 A first attempt with a  $^{36}\text{Cl}$  source prepared on a copper foil and embedded sub-  
197 sequently between two copper–gold bilayers was made; unfortunately, the detector  
198 did not perform as expected and no exploitable spectrum could be measured. New  
199 measurements with both gold and copper–gold bilayer absorbers will be performed  
200 shortly and compared with the Monte Carlo simulations.

## 201 5 Conclusions and Perspectives

202 Within the European Metrology Research Project MetroBeta, developments of both  
203 MMCs and source/absorber preparation techniques for beta spectrometry have been  
204 conducted. Several spectra with end-point energies ranging from  $\sim 76$  to 294 keV  
205 were measured, and the measurements of  $^{36}\text{Cl}$  ( $Q_{\beta} = 709$  keV) are ongoing. It was  
206 demonstrated that MMC measurements also have the potential to yield valuable  
207 information about other decay scheme parameters such as the probability of the beta  
208 decay from  $^{151}\text{Sm}$  to the excited level of  $^{151}\text{Eu}$ . Thus, MMC spectrometry of radio-  
209 nuclides with more complex decay schemes is an interesting extended research field

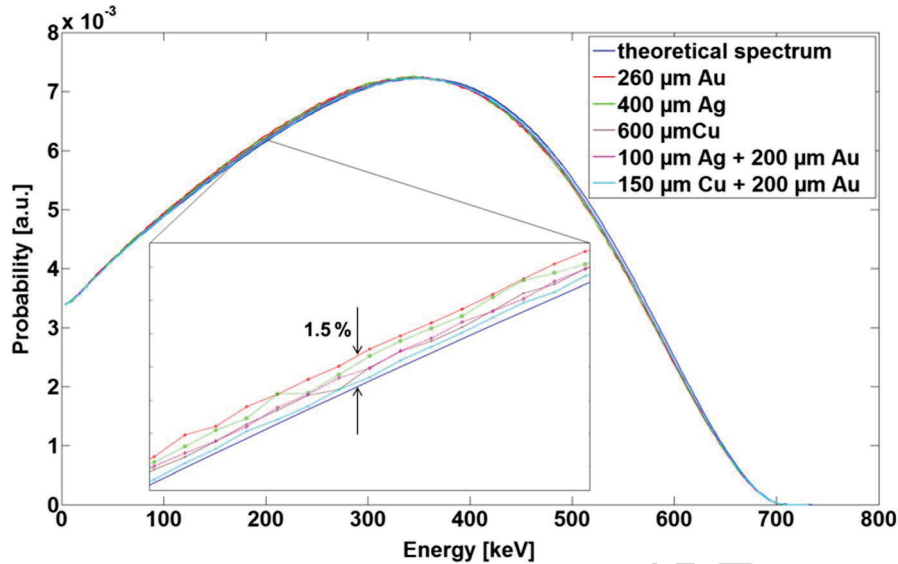


**Fig. 6** Simulation of the spectrum distortion due to the escape of bremsstrahlung in the case of the beta spectrum of  $^{36}\text{Cl}$  ( $Q = 709.53$  keV). The initial spectrum based on Ref. [1] is shown in dark blue. Five types of absorbers were simulated: Au (red), Ag (green), Cu (brown), Ag–Au bilayer (magenta) and Cu–Au bilayer (cyan). The layer thicknesses are indicated in the figure. For better visibility, the inset shows a zoom into the energy range 150–200 keV. (Color figure online)

210 [13]. Studies indicate that  $^{129}\text{I}$ ,  $^{204}\text{Tl}$  and  $^{210}\text{Pb}$  are promising candidates for such  
 211 measurements which should yield valuable nuclear decay data.

212 **Acknowledgements** This work was performed as part of the EMPIR Project 15SIB10 MetroBeta. The  
 213 project has received funding from the EMPIR program co-financed by the Participating States and from  
 214 the European Union's Horizon 2020 research and innovation program.

## 215 References

- 216 1. H. Rotzinger, M. Linck, A. Burck, M. Rodrigues, M. Loidl, E. Leblanc, L. Gastaldo, A. Fleis- AQ4  
 217 chmann, C. Enss, J. Low Temp. Phys. **151**, 1087 (2008)
- 218 2. M. Loidl, M. Rodrigues, B. Censier, S. Kowalski, X. Mougeot, P. Cassette, T. Branger, D. Lacour,  
 219 Appl. Radiat. Isot. **68**, 1454 (2010)
- 220 3. M. Loidl, C. Le-Bret, M. Rodrigues, X. Mougeot, J. Low Temp. Phys. **176**, 1040 (2014)
- 221 4. <http://metrobeta-empir.eu/>
- 222 5. M. Loidl, J. Beyer, L. Bockhorn, C. Enss, D. Györi, S. Kempf, K. Kossert, R. Mariam, O. Nähle, M.  
 223 Paulsen, M. Rodrigues, M. Schmidt, J. Low Temp. Phys. **193**, 1251 (2018)
- 224 6. C. Le-Bret, M. Loidl, M. Rodrigues, X. Mougeot, J. Bouchard, J. Low Temp. Phys. **167**, 985 (2012)
- 225 7. A.S. Hoover et al., Anal. Chem. **87**, 3996–4000 (2015)
- 226 8. X. Mougeot, C. Bisch, Phys. Rev. A **90**, 012501 (2014)
- 227 9. X. Mougeot, Phys. Rev. C **92**, 059902 (2015)
- 228 10. M.-M. Bé et al., Table of Radionuclides, Monographie BIPM-5, vol. 8 (2016),  
 229 ISBN-13 978-92-822-2264-5
- 230 11. M. Reich, H.M. Schüpferling, Z. Phys. **271**, 107–113 (1974)

- 231 12. F. Salvat et al., PENELOPE A code system for Monte Carlo simulation of Electron and Photon  
232 transport, Rapport NEA/NSC/DOC (2001) 19  
233 13. P. C.-O. Ranitzsch, D. Arnold, J. Beyer, L. Bockhorn, J. J. Bonaparte, C. Enss, K. Kossert, S.  
234 Kempf, M. Loidl, R. Mariam, O. J. Nähle, M. Paulsen, M. Rodrigues, M. Wegner, J. Low Temp.  
235 Phys. This Special Issue (2019)  
236 14. S. Kempf, A. Fleischmann, L. Gastaldo, C. Enss, J. Low Temp. Phys. **193**, 365 (2018)

237 **Publisher's Note** Springer Nature remains neutral with regard to jurisdictional claims in published  
238 maps and institutional affiliations.  
239

Journal:	<b>10909</b>
Article:	<b>2398</b>

## Author Query Form

**Please ensure you fill out your response to the queries raised below and return this form along with your corrections**

Dear Author

During the process of typesetting your article, the following queries have arisen. Please check your typeset proof carefully against the queries listed below and mark the necessary changes either directly on the proof/online grid or in the 'Author's response' area provided below

Query	Details Required	Author's Response
AQ1	Kindly check and confirm whether the mail ID is correctly identified.	
AQ2	Kindly check and confirm whether the corresponding author is correctly identified.	
AQ3	Kindly check and confirm the section headings are correctly identified.	
AQ4	As References 1 and 14 are same, we have deleted the duplicate reference and renumbered accordingly. Please check and confirm.	